

Site Preference of Manganese on the Copper Site in Mn-Substituted CuInSe₂ Chalcopyrites Revealed by a Combined Neutron and X-ray Powder Diffraction Study

Jinlei Yao,[†] Zhenxing Wang,[‡] Johan van Tol,[‡] Naresh S. Dalal,[‡] and Jennifer A. Aitken*,[†]

[†]Department of Chemistry and Biochemistry, Duquesne University, Pittsburgh, Pennsylvania 15282, and

[‡]National High Magnetic Field Laboratory, and Department of Chemistry and Biochemistry, Florida State University, Tallahassee, FL 32306

Received September 7, 2009. Revised Manuscript Received December 7, 2009

Ternary chalcopyrite systems are of interest for a number of applications, including host materials for dilute magnetic semiconductors and thin film photovoltaic cells. There are two cation sites, *4a* and *4b*, in the chalcopyrites, and the location of transition-metal ions in the chalcopyrites plays an important role in determining their magnetic and electrical properties. In this work, neutron and X-ray powder diffraction of the Mn-substituted CuInSe₂ compounds, namely, CuIn_{1-x}Mn_xSe₂ (*x* = 0.05 and 0.10) and Cu_{1-y}In_{1-y}Mn_{2y}Se₂ (*y* = 0.05, 0.15, and 0.20), has been carried out. Rietveld refinements using the neutron and X-ray diffraction data reveal a site preference of manganese ions on the copper site (*4a*) rather than the indium site (*4b*), in both series, namely, under In-poor conditions and under Cu-poor and In-poor conditions. The major fraction of Mn ions occupies the copper site, which thus pushes the expelled copper ions to the indium site, resulting in antisite Cu_{In} defects. These results can help to explain why Mn-substituted CuInSe₂ compounds display antiferromagnetic interactions instead of ferromagnetic coupling as predicted by first-principles calculations. High frequency electron paramagnetic resonance measurements suggest that the oxidation state of the manganese ions is divalent.

1. Introduction

Chalcopyrites, such as CuInSe₂, have attracted great attention in recent years, due to their potential applications in next-generation solar cells and spintronic devices.^{1,2} The chalcopyrite structure can be obtained by doubling the unit cell of zincblende along the 4-fold axis (see Figure 1). Chalcopyrites are classified into two groups of compounds based on the constituent elements, that is, I–III–VI₂ and II–IV–V₂. In both systems, there are two cation sites, *4a* and *4b*, which provide potential substitution locations for transition metal (TM) ions.

Some impediments to wide-scale applications of CuInSe₂-based photovoltaic cells are the high cost and low availability of indium. To reduce production costs, some researchers have considered using low-cost TMs, such as zinc and manganese, to replace a significant portion of indium.^{3–5} However, this replacement can have a direct effect on the structural and physicochemical properties of TM-substituted CuInSe₂. Therefore, knowledge of cationic

ordering is a prerequisite to understanding the substitution behaviors and effects.

Moreover, CuInSe₂ and related chalcopyrites have been considered as host materials for dilute magnetic semiconductors (DMSs).^{6–10} The site occupation of the magnetic ions plays a crucial role in determining the conductivity type and magnetic properties in chalcopyrite-type DMSs. For instance, in Mn-doped CuGaSe₂,⁶ the Mn²⁺ ion substituting on the lower-valence-state copper site, Mn_{Cu}, is expected to be an electron donor (n-type), while Mn_{Ga} acts as an acceptor (p-type). Only p-type DMSs are expected to be ferromagnetic based on the theory of hole-mediated ferromagnetism as in GaAs:Mn.¹¹ First-principles calculations on Mn-doped Cu–III–VI₂ chalcopyrites predict that Mn prefers the III site under Cu-rich and III-poor conditions and the Cu site under III-rich conditions.¹² Experimentally, extended X-ray absorption fine structure measurements (EXAFS) on (MnS)_{2x}(CuInS₂)_{1-x} (*x* = 0.02–0.09) compounds indicate the preference of manganese on the indium site.¹³

*Corresponding author. Fax: +1 412 396 5683. E-mail address: aitkenj@duq.edu.

- (1) Stanberry, B. J. *Crit. Rev. Solid State Mater. Sci.* **2002**, *27*, 73.
- (2) Pearton, S. J.; Abernathy, C. R.; Norton, D. P.; Hebard, A. F.; Park, Y. D.; Boatner, L. A.; Budai, J. D. *Mater. Sci. Eng. R* **2003**, *40*, 137.
- (3) Schorr, S.; Tovar, M.; Sheptyakov, D.; Keller, L.; Geandier, G. *J. Phys. Chem. Solids* **2005**, *66*, 1961.
- (4) Schorr, S.; Tovar, M.; Stuesser, N.; Sheptyakov, D.; Geandier, G. *Physica B* **2006**, *385*, 571.
- (5) Yao, J.; Kline, C. N.; Gu, H.; Yan, M.; Aitken, J. A. *J. Solid State Chem.* **2009**, *182*, 2579.
- (6) Zhao, Y. J.; Freeman, A. J. *J. Magn. Magn. Mater.* **2002**, *246*, 145.
- (7) Zhao, Y. J.; Zunger, A. *Phys. Rev. B* **2004**, *69*, 104422.
- (8) Medvedkin, G. A.; Ishibashi, T.; Nishi, T.; Hayata, K.; Hasegawa, Y.; Sato, K. *Jpn. J. Appl. Phys. Part 2 - Lett.* **2000**, *39*, L949.
- (9) Erwin, S. C.; Zutic, I. *Nat. Mater.* **2004**, *3*, 410.
- (10) Aitken, J. A.; Tsoi, G. M.; Wenger, L. E.; Brock, S. L. *Chem. Mater.* **2007**, *19*, 5272.
- (11) Dietl, T.; Ohno, H.; Matsukura, F. *Phys. Rev. B* **2001**, *63*, 195205.
- (12) Zhao, Y. J.; Zunger, A. *Phys. Rev. B* **2004**, *69*, 075208.
- (13) Pietnaczka, A.; Bacewicz, R.; Schorr, S. *Phys. Status Solidi A* **2006**, *203*, 2746.

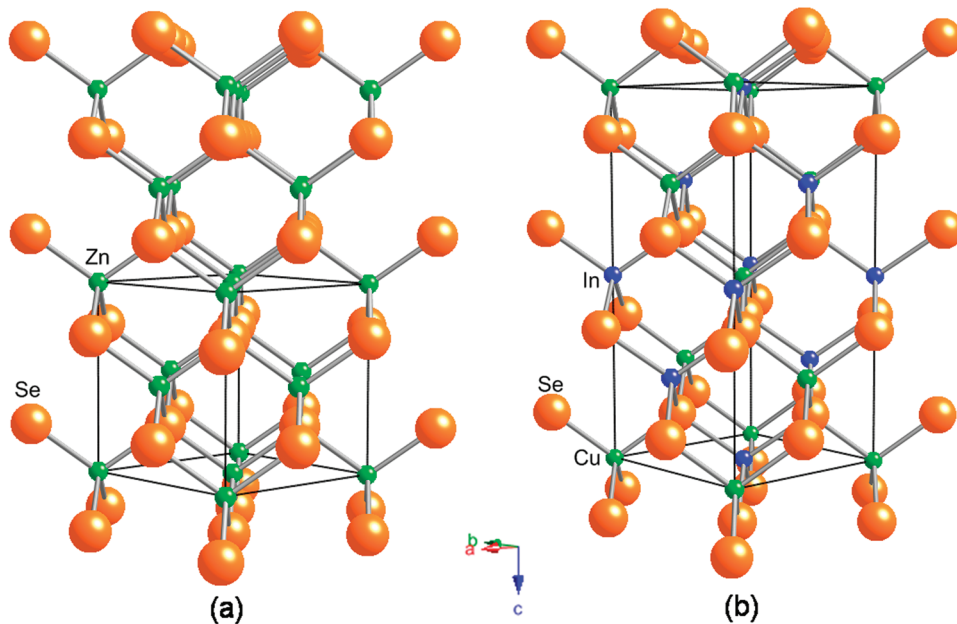


Figure 1. The crystal structure of (a) zincblende-type ZnSe and (b) chalcopyrite-type CuInSe₂.

However, in this work we present clear evidence of the preferential occupation of manganese on the copper site, rather than on the indium site, in the Mn-substituted CuInSe₂ system.

Our previous studies, including thermal analysis and X-ray powder diffraction (XRPD), on the Mn-substituted CuInSe₂ chalcopyrites show that CuIn_{1-x}Mn_xSe₂ and Cu_{1-y}In_{1-y}Mn_{2y}Se₂ can tolerate manganese substitution up to $x = 0.10$ and $2y = 0.20$, respectively, while maintaining phase-pure, chalcopyrite-type materials.⁵ However all Mn-substituted CuInSe₂ chalcopyrites display a paramagnetic behavior rather than a ferromagnetic one.⁵ To understand the underlying physicochemical mechanism of magnetic interaction in this kind of materials, a clear picture of cation ordering and oxidation state of the manganese ions is required. Analysis of XRPD gave us a reliable relationship between lattice parameters and manganese substitution.⁵ However, similar X-ray scattering factors of copper and manganese hamper the differentiation of site occupation of manganese on the cation sites using conventional XRPD. Fortunately, due to the remarkable difference in the neutron scattering lengths of these cations ($b(\text{Cu}) = 7.718 \text{ fm}$, $b(\text{Mn}) = -3.750 \text{ fm}$, and $b(\text{In}) = 4.065 \text{ fm}$),¹⁴ neutron powder diffraction (NPD) provides us with a reliable way to reveal the cationic ordering. Therefore, the structural details, that is, atomic coordinates, cation ordering and thermal parameters, can be obtained accurately by using a combination of XRPD and NPD data. Additionally, electron paramagnetic resonance (EPR) was used to identify the presence of Mn²⁺ in our Mn-substituted CuInSe₂ samples.

2. Experimental Section

2.1. Reagents. The chemicals in this work were used as obtained unless otherwise noted: (i) copper powder, -100 mesh,

99.999%, Strem; (ii) indium powder, -325 mesh, 99.99%, Strem; (iii) manganese chips, $0.8-3$ mm, 99.99%, Cerac; and (iv) selenium powder, -200 mesh, 99.99%, Strem. The manganese pieces were cleaned with hot 10% HNO₃ in methanol and then ground into powder in an argon-filled glovebox.

2.2. Synthesis. Samples with a nominal composition CuIn_{1-x}Mn_xSe₂ ($x = 0.0125$, 0.05 , and 0.10) and Cu_{1-y}In_{1-y}Mn_{2y}Se₂ ($y = 0.05$, 0.15 , and 0.20) were synthesized via high-temperature, solid-state reactions of the constituent elements, similar to a procedure found in the literature.¹⁵ Additionally, an unsubstituted CuInSe₂ sample was prepared for comparison purposes. The elements were weighed, combined and ground for 10 min using an agate mortar and pestle. The mixture was loaded into a relatively short 9 mm o.d. fused-silica tube (4–5 cm) which was then placed into a longer 12 mm o.d. fused-silica tube (13–15 cm) in an argon-filled glovebox. The outer 12 mm o.d. tube was sealed under a vacuum $< 10^{-3}$ mbar using a natural gas/oxygen torch. The samples were heated in the following manner using a programmable furnace: heated to 1000 °C in 24 h, dwelled at 1000 °C for 96 h, and cooled to room temperature in 24 h. After cooling, the polycrystalline samples were removed from the tubes, inspected under an optical microscope, and ground for characterization.

2.3. Physical Measurements. *2.3.1. X-ray Powder Diffraction, Neutron Powder Diffraction, and Rietveld Refinement.* XRPD patterns were collected using a PANalytical X'pert PRO MPD powder X-ray diffractometer with the X'celerator detector operating at 45 kV and 40 mA in the Bragg–Brentano geometry and using Cu K α radiation. Scans were performed from 15 to 145° θ with a step width of 0.008° and a scan speed of 0.010644°/s. Samples were prepared for analysis by grinding the sample powder in an agate mortar and pestle and then back-filling the powder into the aluminum sample holder. Silicon powder from the Gem Dugout was used as an internal standard reference to correct the sample height displacement. Crystalline phases were identified using the search match capabilities of the X'pert HighScore Plus program along with the ICDD

(International Centre for Diffraction Data) powder diffraction file (PDF) database.¹⁶

NPD experiments were conducted on the high-resolution, 32-detector neutron powder diffractometer (BT-1) at the National Institute of Standards and Technology (NIST) Center for Neutron Research, Gaithersburg, MD, with a neutron wavelength of 1.5403(2) Å selected from a Cu (311) monochromator and 15° in-pile collimation at a takeoff angle of 90°. The powder samples (ca. 5 g) were loaded into thin-walled vanadium cans of 50 mm length and 10.8 mm diameter. The NPD data were collected from 3° to 168° 2θ with a step width of 0.05° under ambient conditions.

Rietveld refinements using a combination of XRPD and NPD data were carried out using GSAS with an interface of EXPGUI.^{17,18} Neutron and X-ray diffraction peakshapes were quantified by a Pseudo-Voigt function and a Pseudo-Voigt function with the Finger-Cox-Jephcoat asymmetry correction, respectively. The background was described as a shifted Chebyschev type. The following parameters were refined: scale factor, background parameters, lattice parameters, peak shape parameters, atomic coordinates, isotropic displacement parameters (U_{iso}) and site occupation factors (SOFs). Additionally, zero shift was also fitted for NPD data while sample displacement was only fitted for XRPD data. The chalcopyrite structure of CuInSe₂ was taken as a starting model,¹⁵ and each structural model was refined to convergence.

2.3.2. High Frequency Electron Paramagnetic Resonance. High frequency EPR spectra were recorded at 216 GHz on a home-built EPR spectrometer which is located at the National High Magnetic Field Laboratory in Tallahassee, FL, U.S.A. The spectrometer employs a phase-locked Virginia Diodes microwave source generating a frequency of 13 ± 1 GHz and producing its harmonics of which the 4th, 8th, 16th, 24th, and 32nd were available. A superconducting magnet (Oxford Instruments) capable of reaching a field of 17 T was utilized. Temperature variation was accomplished by using an Oxford continuous helium flow cryostat over the range of 3.6–400 K. A detailed description of the setup is given elsewhere.^{19,20} The EPR spectra were simulated using the EPRCalc program.²¹

3. Results

3.1. XRPD, NPD, and Rietveld Refinement. The polycrystalline CuInSe₂ and Mn-substituted CuInSe₂ ingots synthesized via high-temperature solid-state reactions are grayish black, in agreement with the optical bandgap of 0.9–1.04 eV.^{5,22,23} The XRPD patterns show that all of the ingots discussed here are phase-pure materials with

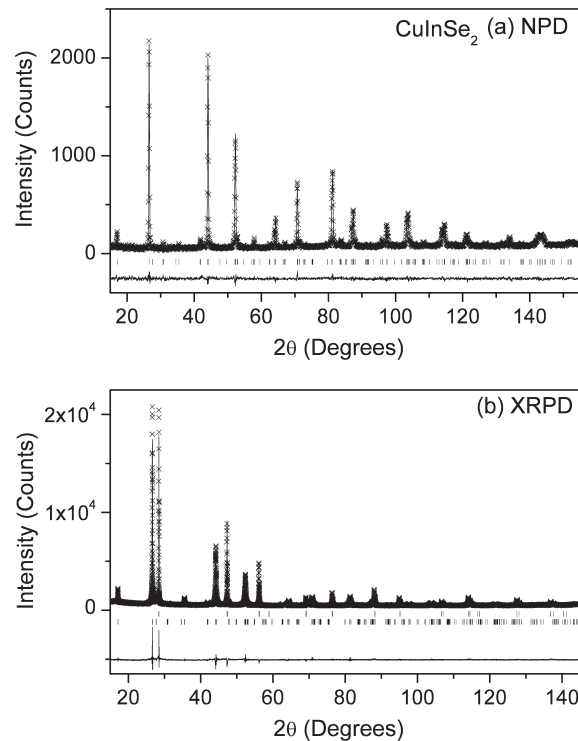


Figure 2. Rietveld refinement using (a) neutron ($wR_p = 0.089$ and $R_p = 0.071$) and (b) X-ray diffraction ($wR_p = 0.0573$ and $R_p = 0.0437$) data for CuInSe₂. The goodness of fit $\chi^2 = 1.992$. Observed (++) and calculated (solid line) neutron/X-ray powder diffraction patterns are shown on the top. The difference between observed and calculated intensities is shown as a difference plot on the bottom. A set of tick marks between the powder diffraction and difference patterns indicate the predicted Bragg reflections of the samples in (a), and of silicon standard and the sample from top to bottom, respectively.

the chalcopyrite structure, in agreement with our previous results and other work in the literature.^{5,24}

As mentioned above, the diamond-like crystal structure of I–III–VI₂ chalcopyrites (space group $\bar{I}\bar{4}2d$) is closely related to that of the zincblende II–VI binary analogues (see Figure 1). The chalcopyrite structure can be considered as a superlattice of the zincblende structure in which half of the cations are replaced by +1 ions and the other half are occupied by +3 ions in an orderly fashion. Therefore, for example, in chalcopyrite-type CuInSe₂, there are two cation sites, Cu on site 4a (0,0,0) and In on site 4b (0,0,0.5), and Se on site 8d (x_{Se} , 0.25, 0.125 with $x_{Se} \sim 0.25$) coordinated by two copper and two indium cations. As is the coordination environment of any ion in a diamond-like structure, each Cu/In cation is tetrahedrally coordinated. The selenium anion is slightly displaced from the ideal zincblende site, which makes the copper cation closer than the indium cation to a small extent. The structural parameters and unit cell parameters, a and c , x_{Se} , and U_{iso} , are required to describe to the crystal structure of unsubstituted CuInSe₂. To define the crystal structure of Mn-substituted CuInSe₂ samples, the SOFs of the cation sites are also needed.

The Rietveld refinement results of unsubstituted CuInSe₂ are illustrated in Figure 2 and Table 1. The lattice parameters and anion x -coordinate determined in this work, $a = 5.7843(1)$ Å, $c = 11.6256(3)$ Å, and

- (16) X. p. H. Plus, *X'pert HighScore Plus*, 2.2, PANalytical B. V.: Almelo, The Netherlands, 2006.
- (17) Larson, A. C.; Von Dreele, R. B. *Los Alamos National Laboratory Report LAUR* **1994**, 86, 748.
- (18) Toby, B. H. *J. Appl. Crystallogr.* **2001**, 34, 210.
- (19) Cage, B.; Hassan, A. K.; Pardi, L.; Krzystek, J.; Brunel, L.-C.; Dalal, N. S. *J. Magn. Reson.* **1997**, 124, 495.
- (20) Hassan, A. K.; Pardi, L. A.; Krzystek, J.; Sienkiewicz, A.; Goy, P.; Rohrer, M.; Brunel, L. C. *J. Magn. Reson.* **2000**, 142, 300.
- (21) Simulations were done using the “EPRCalc” program developed by Johan van Tol at the National High Magnetic Field Laboratory, Tallahassee, FL, U.S.A.
- (22) Horig, W.; Neumann, H.; Sobotta, H.; Schumann, B.; Kuhn, G. *Thin Solid Films* **1978**, 48, 67.
- (23) Shay, J. L.; Tell, B.; Kasper, H. M.; Schiavone, L. M. *Phys. Rev. B* **1973**, 7, 4485.
- (24) Matsushita, H.; Watanabe, M.; Katsui, A. *J. Phys. Chem. Solids* **2008**, 69, 294.

Table 1. Structural Parameters for CuInSe₂ Obtained by Rietveld Refinements

atom	Wyc.	x	y	z	SOF	100U _{iso} (Å ²)
Cu	4a	0	0	0	0.989(5)	2.3(1)
In	4b	0	0	0.5	1	1.57(8)
Se	8d	0.2296(3)	0.25	0.15	0.932(7)	1.03(7)

$x_{\text{Se}} = 0.2296(3)$, are within the range of reported values of $a = 5.780\text{--}5.7877 \text{ \AA}$, $c = 11.609\text{--}11.6464 \text{ \AA}$, and $x_{\text{Se}} = 0.223\text{--}0.235$ for powder or single crystal CuInSe₂ samples.²⁵⁻²⁸ The refined SOFs suggests that the sample is slightly Se-poor (SOF(In) fixed at 1, SOF(Se) = 0.932(7)), in agreement with our inductively coupled plasma (ICP) results.⁵ The ICP measurements show that all the unsubstituted and Mn-doped CuInSe₂ samples are Se-poor and the cationic composition is quite close to the intended stoichiometry.⁵ Considering our ICP results and that the SOF(Cu) (=0.989(5)) deviation from 1 does not exceed the sensitivity of XRPD and NPD, we postulated that both the cation sites, the 4a and 4b sites, are fully occupied for all studied samples.

To elucidate the site occupation of Mn in CuInSe₂, NPD and XRPD experiments of samples in the Cu_{1-y}In_{1-y}Mn_{2y}Se₂ series, which provide the manganese ions equal “opportunity” to occupy both the cation sites, have been carried out. Since all the Mn-substituted CuInSe₂ materials are paramagnetic, only nuclear scattering is observed by NPD. As mentioned above, there are the two cation sites, 4a and 4b, which can be occupied by these three cations, Cu, In, and Mn. For the NPD data, the measured scattering lengths of the 4a and 4b sites, b(4a) and b(4b), are determined by the cation SOFs:

$$\begin{aligned} b(4a) = & \text{SOF(Cu)}_{4a} \cdot b(\text{Cu}) + \text{SOF(Mn)}_{4a} \cdot b(\text{Mn}) \\ & + \text{SOF(In)}_{4a} \cdot b(\text{In}) \end{aligned} \quad (1)$$

and

$$\begin{aligned} b(4b) = & \text{SOF(Cu)}_{4b} \cdot b(\text{Cu}) + \text{SOF(Mn)}_{4b} \cdot b(\text{Mn}) \\ & + \text{SOF(In)}_{4b} \cdot b(\text{In}) \end{aligned} \quad (2)$$

For the XRPD data, we have a similar relationship for the measured X-ray scattering strength, f, of both cation sites:

$$\begin{aligned} f(4a) = & \text{SOF(Cu)}_{4a} \cdot f(\text{Cu}) + \text{SOF(Mn)}_{4a} \cdot f(\text{Mn}) \\ & + \text{SOF(In)}_{4a} \cdot f(\text{In}) \end{aligned} \quad (3)$$

and

$$\begin{aligned} f(4b) = & \text{SOF(Cu)}_{4b} \cdot f(\text{Cu}) + \text{SOF(Mn)}_{4b} \cdot f(\text{Mn}) \\ & + \text{SOF(In)}_{4b} \cdot f(\text{In}) \end{aligned} \quad (4)$$

Based on Rietveld analysis using a combination of XRPD and NPD data of unsubstituted CuInSe₂, both cation

(25) Zahn, G.; Paufler, P. *Cryst. Res. Technol.* **1988**, *23*, 499.
 (26) Merino, J. M.; deVidales, J. L. M.; Mahanty, S.; Diaz, R.; Rueda, F.; Leon, M. *J. Appl. Phys.* **1996**, *80*, 5610.
 (27) Paszkowicz, W.; Lewandowska, R.; Bacewicz, R. *J. Alloys Compd.* **2004**, *362*, 241.
 (28) Knight, K. S. *Mater. Res. Bull.* **1992**, *27*, 161.

sites are assumed to be occupied fully:

$$\text{SOF(Cu)}_{4a} + \text{SOF(Mn)}_{4a} + \text{SOF(In)}_{4a} = 1 \quad (5)$$

and

$$\text{SOF(Cu)}_{4b} + \text{SOF(Mn)}_{4b} + \text{SOF(In)}_{4b} = 1 \quad (6)$$

Considering the limitation caused by the similar X-ray scattering strengths of copper and manganese and the ICP-measured manganese content being close to the intended one, the sum of manganese occupancies in both sites is constrained to the nominal composition:

$$\text{SOF(Mn)}_{4a} + \text{SOF(Mn)}_{4b} = 2y \quad (7)$$

Based on these assumptions and eqs 1–7, Model A, (Cu, Mn, In)_{4a}(In, Mn, Cu)_{4b}(Se_{2- δ})_{8d}, in which the cation sites are fully occupied by copper, manganese, and indium, while selenium anions exclusively occupy the 8d site, was proposed and refined using the combination of XRPD and NPD data of Cu_{1-y}In_{1-y}Mn_{2y}Se₂ compounds (see Table 2). The Rietveld refinement suggests an existence of a manganese preference for the 4a site in the Cu_{1-y}In_{1-y}Mn_{2y}Se₂ system, for example, SOF(Mn)_{4a} = 0.048(7) vs SOF(Mn)_{4b} = 0.02(7) for the sample with 2y = 0.05. The refined chemical formula using this model is slightly lower in copper and selenium content and higher in indium content compared to the nominal composition, for example, Cu_{0.915}In_{0.942}Mn_{0.15}Se_{1.91} vs Cu_{0.925}In_{0.925}Mn_{0.15}Se₂ for the sample with 2y = 0.15. The Se-poor characteristic of these samples is in good agreement with our previous ICP measurements;⁵ however, the Cu-poor and In-rich characteristic derived from this Rietveld refinement is in contrast to the results of ICP.

The Cu-deficiency indicated by the refinement of Model A may suggest that the remaining copper ions occupy interstitial sites, which cannot be detected using conventional powder diffraction techniques. Taking into account Mn preferential occupation on the 4a site, it is most likely that copper ions occupy the other cation site, that is, the 4b site, in the chalcopyrite structure. The assignment of the remaining copper on the 4b site increased the total copper content and decreased the SOF of indium on this site, resulting in the refined composition complying with the intended one. Based on this consideration, the indium ions are only placed on the 4b site and fixed to the nominal content:

$$\text{SOF(In)}_{4a} = 0 \quad \text{and} \quad \text{SOF(In)}_{4b} = 1 - y \quad (8)$$

From eqs 5–8, another equation is implied

$$\text{SOF(Cu)}_{4a} + \text{SOF(Cu)}_{4b} = 1 - y \quad (9)$$

suggesting that the sum of copper in both sites is constrained as the nominal composition. According to this assumption, the model was adjusted to Model B, (Cu, Mn)_{4a}(In, Mn, Cu)_{4b}(Se_{2- δ})_{8d}, in which the 4a site is fully occupied by Cu and Mn ions, and copper ions share the

Table 2. Structural Parameters and Refinement Details for $\text{Cu}_{1-y}\text{In}_{1-y}\text{Mn}_{2y}\text{Se}_2$ Compounds Obtained by Rietveld Refinements

parameters	$2y = 0.05$		$2y = 0.15$		$2y = 0.20$	
	Model A ^a	Model B ^a	Model A ^a	Model B ^a	Model A ^a	Model B ^a
Cation 4a						
SOF(Cu)	0.948(7)	0.963(7)	0.889(4)	0.905(4)	0.858(7)	0.894(6)
SOF(Mn)	0.048(7)	0.037(7)	0.092(4)	0.095(4)	0.111(7)	0.106(6)
SOF(In)	0.004(12)	0	0.02(1)	0	0.03(1)	0
$100U_{\text{iso}} (\text{\AA}^2)$	1.9(1)	2.2(1)	2.13(9)	1.98(7)	2.3(1)	2.34(9)
Cation 4b						
SOF(In)	1.031(7)	0.975	0.916(8)	0.925	0.94(1)	0.9
SOF(Mn)	0.02(7)	0.013(7)	0.058(4)	0.055(4)	0.089(7)	0.094(6)
SOF(Cu)	-0.03(2)	0.012(7)	0.02(1)	0.020(4)	-0.03(1)	0.006(6)
$100U_{\text{iso}} (\text{\AA}^2)$	1.89(9)	1.84(8)	2.41(7)	2.51(7)	1.18(7)	1.26(7)
Anion 8d						
SOF(Se)	0.96(1)	0.927(7)	0.955(7)	0.967(6)	0.98(1)	0.970(7)
$100U_{\text{iso}} (\text{\AA}^2)$	1.43(9)	1.29(7)	1.31(4)	1.32(4)	1.36(6)	1.29(6)
x_{Se}	0.2289(3)	0.2290(3)	0.2303(2)	0.2304(2)	0.2307(3)	0.2308(3)
Reliability Factors						
χ^2	1.557	1.559	1.755	1.758	1.761	1.762
wR_p (NPD)	0.0791	0.0792	0.0519	0.0521	0.0882	0.0883
R_p (NPD)	0.0620	0.0620	0.0416	0.0417	0.0694	0.0696
wR_p (XRPD)	0.0588	0.0589	0.0528	0.0529	0.0538	0.0538
R_p (XRPD)	0.0454	0.0454	0.0408	0.0409	0.0412	0.0412

^a Model A: $(\text{Cu},\text{Mn},\text{In})_{4a}(\text{In},\text{Mn},\text{Cu})_{4b}(\text{Se}_{2-\delta})_{8d}$. Model B: $(\text{Cu},\text{Mn})_{4a}(\text{In},\text{Mn},\text{Cu})_{4b}(\text{Se}_{2-\delta})_{8d}$.

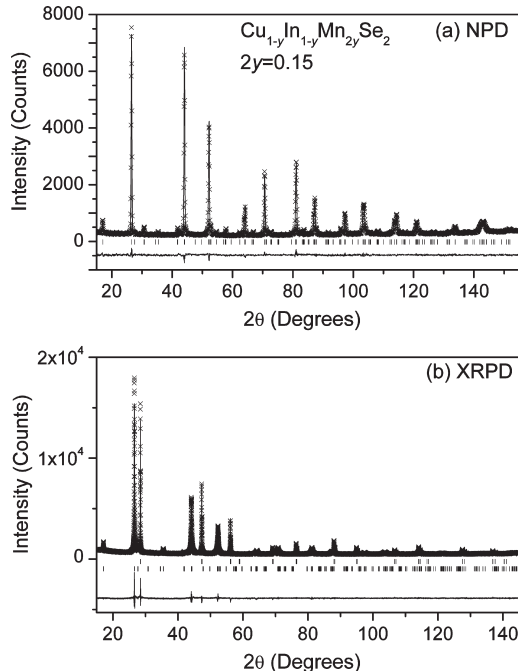


Figure 3. Rietveld refinement using (a) neutron ($wR_p = 0.0521$ and $R_p = 0.0417$) and (b) X-ray diffraction ($wR_p = 0.0529$ and $R_p = 0.0409$) data for $\text{Cu}_{1-y}\text{In}_{1-y}\text{Mn}_{2y}\text{Se}_2$ with $2y = 0.15$ based on the $(\text{Cu},\text{Mn})_{4a}(\text{In},\text{Mn},\text{Cu})_{4b}(\text{Se}_{2-\delta})_{8d}$ model. The goodness of fit $\chi^2 = 1.758$. Observed (++) and calculated (solid line) neutron/X-ray powder diffraction patterns are shown on the top. The difference between observed and calculated intensities is shown as a difference plot on the bottom. A set of tick marks between the powder diffraction and difference patterns indicate the predicted Bragg reflections of the samples in (a), and of silicon standard and the sample from top to bottom, respectively in (b).

4b site with In and Mn ions. The final refinement (see Figure 3) based on Model B also suggests that the samples are Se-poor and the site preference of manganese on the copper site, for example, $\text{SOF}(\text{Mn})_{4a} = 0.037(7)$ vs $\text{SOF}(\text{Mn})_{4b} = 0.013(7)$ for the sample with $2y = 0.05$

(see Table 2), in good agreement with the general results obtained from Model A. Moreover, the Rietveld analysis indicates Cu–In antisite occupation, Cu_{In} , for example, $\text{SOF}(\text{Cu})_{4b} = 0.020(4)$ for the sample with $2y = 0.15$. It can be envisaged that a majority of the manganese ions replaces the copper ions on the 4a site, which thus forces these expelled copper ions into the indium site, forming of the antisite Cu_{In} defect. Cation antisite occupation is a common type of defect found in chalcopyrites and their doped systems.^{3,4} These results suggest that manganese prefers the copper site rather than the indium site in the $\text{Cu}_{1-y}\text{In}_{1-y}\text{Mn}_{2y}\text{Se}_2$ series, that is, under heavily Cu-poor and In-poor conditions.

To verify the above result, namely, site preference of manganese on the copper site, NPD and XRPD experiments on the In-poor $\text{CuIn}_{1-x}\text{Mn}_x\text{Se}_2$ system have been carried out at room temperature. In-poor conditions are expected to result in the substitution of manganese ions on the indium site according to some reported theoretical and experimental results.^{6,12,13} The two models, Models A and B, were applied to the $\text{CuIn}_{1-x}\text{Mn}_x\text{Se}_2$ system. Considering the different composition of $\text{CuIn}_{1-x}\text{Mn}_x\text{Se}_2$, the constraints on chemical composition should be adjusted and thus eqs 7 and 8 were replaced by

$$\text{SOF}(\text{Mn})_{4a} + \text{SOF}(\text{Mn})_{4b} = x \quad (10)$$

and

$$\text{SOF}(\text{In})_{4a} = 0 \quad \text{and} \quad \text{SOF}(\text{In})_{4b} = 1 - x \quad (11)$$

The composition constraints based on eqs 5, 6, 10 and 11 imply that the sum of copper on both cation sites is fixed at unity, that is,

$$\text{SOF}(\text{Cu})_{4a} + \text{SOF}(\text{Cu})_{4b} = 1 \quad (12)$$

Table 3. Structural Parameters and Refinement Details for CuIn_{1-x}Mn_xSe₂ Compounds Obtained by Rietveld Refinements

parameters	<i>x</i> = 0.05		<i>x</i> = 0.10	
	Model A ^a	Model B ^a	Model A ^a	Model B ^a
Cation 4a				
SOF(Cu)	0.935(8)	0.956(7)	0.890(8)	0.937(8)
SOF(Mn)	0.53(8)	0.044(7)	0.081(8)	0.063(8)
SOF(In)	0.01(1)	0	0.03(1)	0
100 <i>U</i> _{iso} (Å ²)	2.1(1)	2.4(1)	1.9(1)	2.5(1)
Cation 4b				
SOF(In)	0.996(8)	0.95	1.013 (8)	0.9
SOF(Mn)	-0.003(8)	0.006(7)	0.019(8)	0.037(8)
SOF(Cu)	0.01(2)	0.044(7)	-0.03(2)	0.063(8)
100 <i>U</i> _{iso} (Å ²)	2.1(1)	2.15(9)	2.06(9)	2.03(9)
Anion 8d				
SOF(Se)	0.97(1)	0.941(7)	0.99(1)	0.931(7)
100 <i>U</i> _{iso} (Å ²)	1.22(9)	1.10(7)	1.57(9)	1.29(7)
<i>x</i> _{Se}	0.2287(3)	0.2288(3)	0.2299(3)	0.2302(2)
Reliability Factors				
χ^2	1.441	1.441	2.091	2.096
<i>wR</i> _p (NPD)	0.0790	0.0791	0.0886	0.0891
<i>R</i> _p (NPD)	0.0626	0.0626	0.0690	0.0690
<i>wR</i> _p (XRPD)	0.0555	0.0555	0.0585	0.0585
<i>R</i> _p (XRPD)	0.0434	0.0434	0.0443	0.0443

^aModel A: (Cu,Mn,In)_{4a}(In,Mn,Cu)_{4b}(Se_{2-*δ*})_{8d}. Model B: (Cu, Mn)_{4a}(In,Mn,Cu)_{4b}(Se_{2-*δ*})_{8d}.

The refinement results using the XRPD and NPD data based on both models are given in Table 3. It can be seen that the results of CuIn_{1-x}Mn_xSe₂ confirms the same structure and composition characteristics of Cu_{1-y}In_{1-y}Mn_{2y}Se₂, that is, Se-poor, manganese preferring the copper site and antisite Cu_{In} occupation. The results found in this system unveil the existence of Mn on the copper site with preference even under In-poor conditions, in disagreement with the previous theoretical prediction and experimental results.^{12,13} The first-principles calculations and EXAFS on Mn-substituted Cu-In-VI₂ (VI = S, Se) chalcopyrites suggest that Mn prefers the indium site under In-poor conditions.^{12,13}

3.2. High Frequency EPR. To determine the oxidation state of the Mn ion, high frequency EPR was utilized to indentify the existence of Mn²⁺ and/or Mn³⁺. Mn²⁺ is expected to have spin *S* = 5/2 with a small zero field splitting (D) while Mn³⁺ has spin *S* = 2 with orders of magnitude larger D value arising from the Jahn-Teller effect.²⁹ Figure 4 shows the EPR spectra of CuIn_{0.9875}Mn_{0.0125}Se₂ and CuIn_{0.95}Mn_{0.05}Se₂ at 216 GHz and 10 K. The spectrum of CuIn_{0.95}Mn_{0.05}Se₂ (Figure 4b) exhibits dipolar broadening of all the peaks due to the high manganese concentration. Since the EPR spectrum of CuIn_{0.95}Mn_{0.05}Se₂ is much less resolved, the following EPR measurements and analysis were performed on the CuIn_{0.9875}Mn_{0.0125}Se₂ sample. Figure 5 shows the EPR spectra of CuIn_{0.9875}Mn_{0.0125}Se₂ at 216 GHz over the range of 5–300 K. The spectra have a single peak at higher temperatures, but additional features develop below ~50 K. At 5 K, the spectrum consists of several

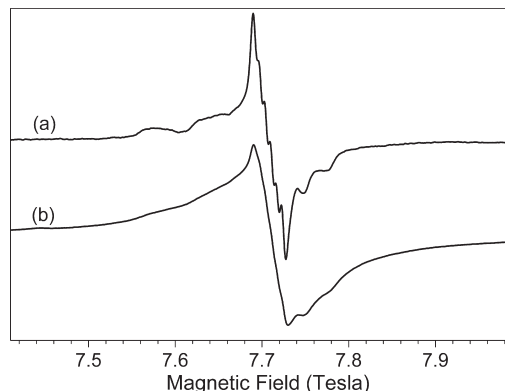


Figure 4. Electron paramagnetic resonance spectra of polycrystalline (a) CuIn_{0.9875}Mn_{0.0125}Se₂ and (b) CuIn_{0.95}Mn_{0.05}Se₂ compounds at 216 GHz and 10 K.

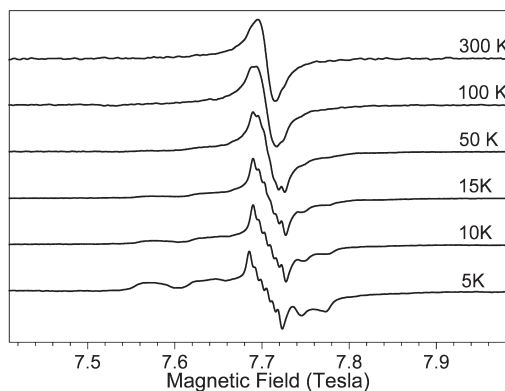


Figure 5. Electron paramagnetic resonance spectra of polycrystalline CuIn_{0.9875}Mn_{0.0125}Se₂ at 216 GHz and various temperatures.

peaks around *g* = 2 field (7.7164 T), implying the existence of Mn hyperfine splitting (A) as well as D. No other peaks were seen beyond the range shown in the figure. The loss of hyperfine splitting at temperatures higher than 100 K implies the emergence of exchange interaction between the various Mn centers, probably mediated by thermally excited charge carriers.

To understand the EPR spectra, we utilized the following Hamiltonian:

$$\hat{H} = \beta g \vec{B} \cdot \vec{S} + D(S_z^2 - S^2/3) + E(S_x^2 - S_y^2) + A \vec{S} \cdot \vec{I} \quad (13)$$

where β stands for the Bohr magneton. Figure 6 shows the experimental spectrum at ~5.5 K. This spectrum cannot be simulated satisfactorily with a single set of zero-field splitting parameters D and E, but a reasonable result is obtained by a simulation with two resolved Mn²⁺ sites and a background of unresolved Mn²⁺ sites. Site 1 has $D = 0.061 \text{ cm}^{-1}$, site 2 has $D = -0.0165 \text{ cm}^{-1}$, and $E = 0.0025 \text{ cm}^{-1}$. The sum of the spectra of these two sites at this low temperature cannot account for the relatively large amplitude in the center of the spectrum which corresponds to the $m_s = -1/2$ to the $m_s = +1/2$ transition. The addition of a third component with a Gaussian distribution of D values with a standard deviation (ΔD) of 0.04 cm^{-1} around $D = 0$ significantly improves the

(29) Abragam, A.; Bleaney, B. *Electron Paramagnetic Resonance of Transition Ions*; Dover Publications: New York, 1986.

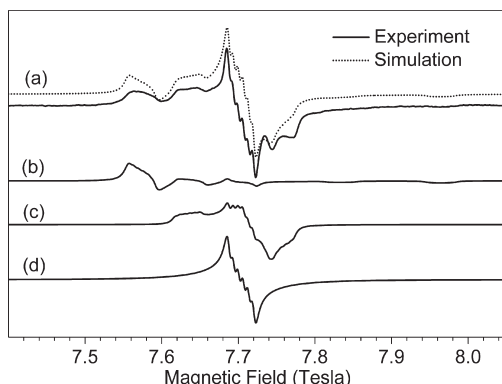


Figure 6. Electron paramagnetic resonance spectrum of polycrystalline $\text{CuIn}_{0.9875}\text{Mn}_{0.0125}\text{Se}_2$ and its simulations: (a) solid line: experiment at 216 GHz and ~ 5.5 K; dotted line: simulation at the same condition, obtained by adding parts (b), (c), and (d); (b) simulation using the following set of spin Hamiltonian parameters: $S = 5/2$, $g = 2.003$, $I = 5/2$, $A = 64.6$ G, and $D = 0.061$ cm^{-1} ; (c) simulation using $S = 5/2$, $g = 2.003$, $I = 5/2$, $A = 64.6$ G, $D = -0.0165$ cm^{-1} , and $E = 0.0025$ cm^{-1} ; (d) simulation using $S = 5/2$, $g = 2.003$, $I = 5/2$, $A = 64.6$ G, $D = 0$ cm^{-1} ($\Delta D = 0.04$ cm^{-1}).

simulation. This term is likely due to various other sites with different local surroundings (neighboring Mn^{2+} substitutions, Cu–In antisites, etc). The small D -values and hyperfine splitting typical of Mn^{2+} in II–VI compounds show that the EPR spectrum is related to Mn^{2+} rather than Mn^{3+} .³⁰ Also, no signals related to Cu^{2+} were found. The three components have similar intensities, and unfortunately the poor resolution at higher Mn concentrations prohibits an analysis of relative intensity of the sites as a function of Mn concentration.

4. Discussion

Our previous XRPD studies on $\text{CuIn}_{1-x}\text{Mn}_x\text{Se}_2$ suggested that the samples have notable Cu vacancy when the $4a$ site is occupied only by copper ions, and indium ions share the $4b$ site with manganese ions.⁵ Attempts to arrange both Mn and Cu on the $4a$ site lead to divergence of the refinement of the X-ray powder data because of the similar X-ray scattering power of Mn and Cu.⁵ As a result of the significant difference in the neutron scattering length of these cations, we utilized the combination of XRPD and NPD techniques to get a clear picture of cation distribution on the crystallographic sites of Mn-substituted CuInSe_2 . Additionally the Rietveld refinements and ICP data indicate the samples to be Se-deficient. However, our analyses cannot rule out the existence of slightly Cu-poor Mn-substituted CuInSe_2 phases. The possible Cu deficiency and the determined Se deficiency may induce amorphous or secondary Cu–Se phases that aggregate at the grain boundaries as in the CuInSe_2 films.³¹ The amount of these secondary phases would be too small to detect by powder diffraction techniques and chemical composition analysis.

(30) Hofmann, A.; Graf, C.; Boeglin, C.; Rühl, E. *ChemPhysChem* **2007**, *8*, 2008.

(31) Yoon, S.; Kim, S.; Craciun, V.; Kim, W. K.; Kaczynski, R.; Acher, R.; Anderson, T. J.; Crisalle, O. D.; Li, S. S. J. *J. Cryst. Growth* **2005**, *281*, 209.

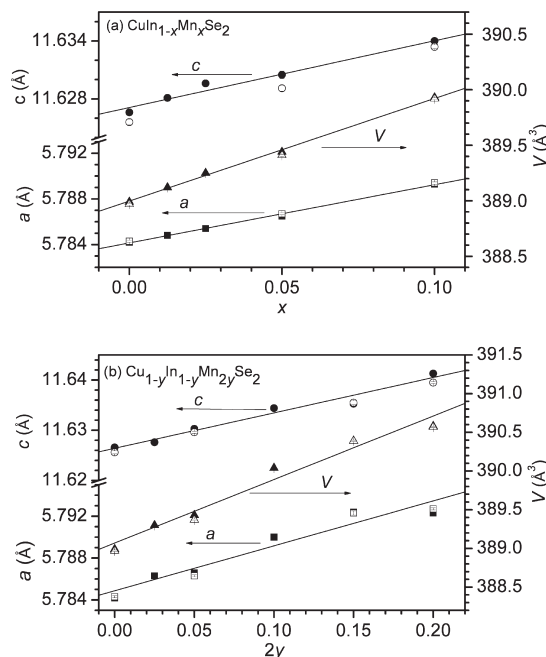


Figure 7. Manganese concentration versus lattice parameters and volume for (a) $\text{CuIn}_{1-x}\text{Mn}_x\text{Se}_2$ and (b) $\text{Cu}_{1-y}\text{In}_{1-y}\text{Mn}_{2y}\text{Se}_2$ compounds. The close/open symbols denote the lattice parameters analyzed from the X-ray/combination of X-ray and neutron diffraction data. The lines are the linear fit to the lattice parameters obtained from the X-ray diffraction data in ref 5.

The lattice parameters of both systems obtained from NPD and XRPD experiments are shown in Figure 7.⁵ It can be seen that the lattice parameters obtained from both experiments are reasonably comparable and follow Vegard's law,³² a linear relationship of the lattice parameters with increasing manganese content, indicating the Mn ions are incorporated into the host cell randomly. However, the fulfillment of Vegard's law cannot ensure that all Mn ions simply occupy the crystallographic sites; there could exist native defects for some portion of manganese.

In the (Ga,Mn)As system, it has been found that the linear increase of lattice parameters with increasing Mn content is a resulting contribution from the substitution of Mn on the Ga site, Mn_{Ga} , interstitial Mn, Mn_{I} , and As antisite defects.³³ The experiments of channeling Rutherford backscattering and particle-induced X-ray emission on highly-Mn-doped (Ga,Mn)As showed that a portion of Mn ($\sim 17\%$ of total manganese content) occupies interstitial, rather than substitutional, sites in the host cell.³⁴ In our Mn-substituted CuInSe_2 samples, there may also exist Mn_{I} donors compensating the acceptors, especially for the samples with greater Mn content. However, it is noteworthy to mention that the major portion of Mn ($\sim 80\%$ of the total manganese content) should occupy the cation sites, assuming our Mn-substituted CuInSe_2 samples have a comparable amount of Mn_{I} defects as in (Ga,Mn)As. Comparing the SOF(Mn)

(32) Vegard, L. *Z. Phys.* **1921**, *5*, 17.

(33) Mašek, J.; Kudrnovský, J.; Máca, F. *Phys. Rev. B* **2003**, *67*, 153203.

(34) Yu, K. M.; Walukiewicz, W.; Wojtowicz, T.; Kuryliszyn, I.; Liu, X.; Sasaki, Y.; Furdyna, J. K. *Phys. Rev. B* **2002**, *65*, 201303.

Table 4. Site Occupancy of Manganese in the Mn-Substituted CuInSe₂ Samples Based on the (Cu,Mn)_{4a}(In,Mn,Cu)_{4b}(Se_{2-δ})_{8d} Model

samples	Mn _{Cu}	Mn _{In}	%Diff [*]
Cu _{1-y} In _{1-y} Mn _{2y} Se ₂	2y = 0.05	0.037	48%
	2y = 0.15	0.095	27%
	2y = 0.20	0.106	6%
CuIn _{1-x} Mn _x Se ₂	x = 0.05	0.044	76%
	x = 0.10	0.063	26%

* %Diff = (Mn_{Cu} - Mn_{In})/(Mn_{Cu} + Mn_{In}) × 100%.

on the cation sites based on Model B (see Tables 2 and 3), one can obtain a large difference between the SOF of Mn_{Cu} and Mn_{In} (see Table 4). For example, for CuIn_{1-x}Mn_xSe₂ with x = 0.05, SOF(Mn) on the 4a site is 76% greater than that on the 4b site. Considering such a significant difference of SOF(Mn) between the cation sites, we believe the existence of native defects, such as Mn_I and antisite defects, may change the relative value of SOF(Mn) on the cation sites; however, it has little possibility to reverse the trend of preferential occupation of Mn on the 4a site. Interestingly, the difference between the SOF of Mn_{Cu} and Mn_{In} reduces as manganese content increases (see Table 4), for example, from 76% for x = 0.05 to 26% for x = 0.10 in the CuIn_{1-x}Mn_xSe₂ series. This suggests that the samples with greater Mn content need more Mn_{In} acceptors compensating the Mn_{Cu} donors; however, it does not change the tendency of Mn_{Cu} preference in Mn-substituted CuInSe₂.

Since Mn-substituted CuInVI₂ (VI = S, Se) compounds display paramagnetic behavior with short-range antiferromagnetic interactions rather than predicted ferromagnetic properties, the superexchange Mn-anion-Mn interaction was proposed to explain the antiferromagnetic coupling.^{5,35} The anion-Mn distance and bond angle in the Mn-anion-Mn pathway are expected to have a direct influence on this exchange process. Therefore careful examination of crystallographic details of Mn-substituted CuInSe₂ was carried out. Figure 8 shows the dependence of the mean cation-Se distance, d_{C-Se}, on the Mn content, x_{Mn}, in Mn-substituted CuInSe₂, including the CuIn_{1-x}Mn_xSe₂ and Cu_{1-y}In_{1-y}Mn_{2y}Se₂ series. The mean cation-Se distance is taken as the average value of 4a-Se and 4b-Se distances, derived from our structure models refined by Rietveld analysis using XRPD and NPD data on Mn-substituted CuInSe₂.⁵ A linear relationship exists between d_{C-Se} and Mn content as follows

$$d_{C-Se} = 2.5106 + 0.0188 \cdot x_{Mn} \text{ \AA} \quad (14)$$

If x_{Mn} is extended to 2 (there are two cation sites in chalcopyrites) according to eq 14, one obtains the Mn-Se distance in the tetrahedral environment to be d_{C-Se} = 2.548 Å, close to the Mn-Se bond length of 2.557 Å derived from the Mn-doped II-Se (II = Zn, Cd, Hg) zincblende/wurtzite phases.³⁶ The determined Mn-Se distance, 2.548 Å, is longer by ~4% than the Cu-Se distance,

(35) Tsujii, N.; Kitazawa, H.; Kido, G. *Phys. Status Solidi A* **2002**, *189*, 951.

(36) Yoder-Short, D. R.; Debska, U.; Furdyna, J. K. *J. Appl. Phys.* **1985**, *58*, 4056.

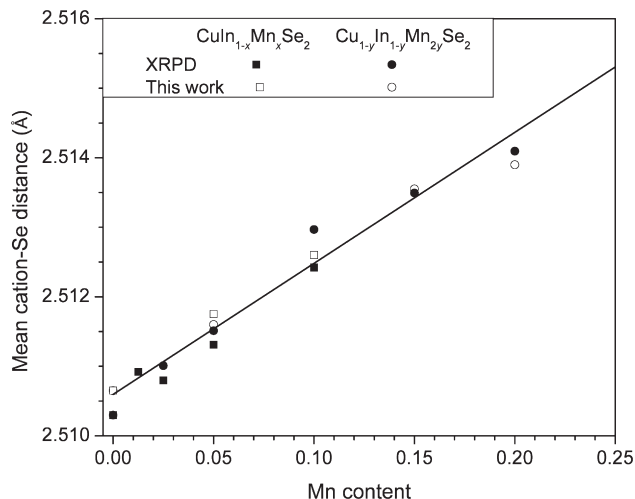


Figure 8. Mean cation-Se distance vs manganese concentration for CuIn_{1-x}Mn_xSe₂ and Cu_{1-y}In_{1-y}Mn_{2y}Se₂ compounds derived from Rietveld refinements using a combination of X-ray and neutron powder diffraction (XRPD and NPD) experiments. The line is the linear fit to the average cation-Se distance of Mn-substituted CuInSe₂.

2.445 Å, and shorter than the In-Se distance, 2.578 Å, in our unsubstituted CuInSe₂ sample. This indicates that Mn prefers the Cu site, since the mixture of the longer Mn-Se bond with the shorter Cu-Se bond results in elongating the bond length of 4a-Se and thus expanding the unit cell, while the mixture of the Mn-Se and In-Se bonds would shrink the crystal lattice. The actual cation-Se bond lengths, Mn-Se, Cu-Se, and In-Se, could be measured in the future using local structure measurements, such as EXAFS. Several batches of the Mn-substituted CuInSe₂ samples have been prepared, and their lattice-parameter refinement, simply based on the space group and without recourse to the specific structure model, yielded the same trend of lattice expansion with the Mn dopant incorporation.

The incorporation of Mn into CuInSe₂ may give rise to the issue of charge balance in these compounds. The oxidation state of selenium is considered as 2- due to no Se-Se bonds in chalcopyrites, and copper/indium can be assigned as 1+/3+ as in most cases of chalcopyrites.^{37,38} The oxidation state of manganese can be 2+ or 3+ in a selenide environment, and we tend to consider it as 2+, confirmed by our EPR data. On the basis of these designations, the charge is slightly off balance, for example (Cu_{0.937}⁺Mn_{0.063}²⁺)_{4a}(In_{0.9}⁺Mn_{0.037}²⁺Cu_{0.063}⁺)_{4b}⁻(Se_{1.862}²⁻)_{8d}(+3.9/-3.7) for the sample with x = 0.10 based on Model B. The unbalance of charge may be due to our assumption that the cation sites are fully occupied. One way to balance charges is to take native defects into account. The defects which may be present as copper (V_{Cu}) or indium vacancies (V_{In}) could act as acceptors to compensate the donors, selenium vacancy (V_{Se}), and Mn_I, leading to charge balance.

(37) Nakai, I.; Izawa, M.; Sugitani, Y.; Niwa, Y.; Nagashima, K. *J. Mineral.* **1975**, *8*, 135.

(38) Pearce, C. I.; Patrick, R. A. D.; Vaughan, D. J.; Henderson, C. M. B.; van der Laan, G. *Geochim. Cosmochim. Acta* **2006**, *70*, 4635.

5. Conclusion

In summary, neutron diffraction is a suitable tool to study the manganese site occupation in Mn-substituted CuInSe₂ materials due to the considerable difference in the neutron scattering lengths of manganese, copper and indium cations. Rietveld refinements using combined XRPD and NPD data reveal that the manganese ions occupy the copper site preferentially under In-poor conditions or under Cu-poor and In-poor conditions. The site preference of manganese on the copper site forces the expelled copper to occupy the indium site, creating anti-site Cu_{In} occupation. High frequency EPR measurements suggest that the oxidation state of Mn is divalent rather than trivalent.

In some cases, experimental work with DMSs agrees with theory and in other instances it does not. Careful studies in several systems have shown that desired/predicted properties can occur for the wrong reasons. For example, magnetic impurity phases, MnP in CdSnP₂ chalcopyrites or ZnFe₂O₄ in Fe- and Cu-doped ZnO, have been found.^{10,39} In this case, we obtain materials that do not have the predicted ferromagnetic properties, probably due in large part to the unexpected site location

(39) Shim, J. H.; Hwang, T.; Lee, S.; Park, J. H.; Han, S.-J.; Jeong, Y. H. *Appl. Phys. Lett.* **2005**, 86, 082503.

of Mn. One should note, however, that the site occupation of Mn could possibly be influenced using different thermal treatments⁴⁰ or nonequilibrium preparation methods, such as rapid solidification, hot press, and so forth. These results presented here supply detailed structural information to improve the computational models, which move forward an understanding of the underlying relationship between crystal structure, composition and physico-chemical properties in the chalcopyrite-type DMSs.

Acknowledgment. This work was supported by the National Science Foundation (NSF) CAREER Award under Grant No. DMR-0645304, and the powder X-ray diffractometer was purchased with funds from the NSF, Grant No. DUE-0511444. We acknowledge the support of NIST, U.S. Department of Commerce, in providing the neutron research facilities used in this work with a proposal No. D24-07. The authors thank Dr. Mark Green and Dr. Hui Wu at NIST for their helpful assistance in the neutron diffraction application and experiment. The NHMFL is funded by the NSF through the Cooperative Agreement No. DMR-0654118, the State of Florida, and the DOE.

(40) Edmonds, K. W.; Boguslawski, P.; Wang, K. Y.; Campion, R. P.; Novikov, S. N.; Farley, N. R. S.; Gallagher, B. L.; Foxon, C. T.; Sawicki, M.; Dietl, T.; Nardelli, M. B.; Bernholc, J. *Phys. Rev. Lett.* **2004**, 92, 037201.